

Enhancing the thermal performance of a phase change energy storage assisted ventilation system via unit structure optimization for data center

Hongli Xu[a], Jiri Zhou[b], Xing Liang[c], Xiaoyan Yi[a], Hongwei Wu[d], Ruiyong Mao[a], Zujing Zhang[a]*
[a] College of Civil Engineering, State Key Laboratory of Public Big Data, Guizhou University, Guiyang 550025, China
[b] China MCC5 Group CORP.LTD., MCC5 Tower, No. 9 Wuye Road, Jinjiang District, Chengdu, 610000, China
[c] School of Computer Science and Mathematics, Kingston University London, KT1 2EE, United Kingdom
[d] School of Physic, Engineering and Computer Science, University of Hertfordshire, Hatfield, AL10 9AB, United Kingdom.
*Corresponding author: Tel: +86 185 2391 9513 Email: zjzhang3@gzu.edu.cn.

Abstract: This numerical study aims to improve the melting uniformity of the phase change plate (PCP) by optimizing structure, enhancing the energy efficiency of PCP's application in the ventilation system of data centers. The anterior-to-posterior slope ratio (W_r), fin configuration, and volume of the PCP are optimized. For the practical application of the PCP with an optimized structure and configuration, the effects of ambient temperature, air supply velocity, phase change temperature and thermal conductivity have been studied. The main results are as follows: (i) When the PCP changes from a rectangular body to a trapezoidal body, the uniformity of melting is improved by 93%. The average cooling range of PCP increases by 0.5℃, and the energy-saving rate increases by 22%. (ii) The structure of the PCP with the volume of 19 L, a W_r of 1.5 and double fin arranged horizontally parallel to the PCP effectively shorts the charging time from 14 h to 11.6 h. (iii) A nonlinear functional relationship between the cooling performance of the system and the main four variables is proposed. This work provides guidelines for the application of PCP in data center.

Keywords: Phase change energy storage; Free cooling; Structure optimization; Ventilation system; Energy conservation; Data centers

Nomenclature

T	Temperature, °C	g	Gravity， m/s^2
T_{in}, T_{out}	Area average air temperature at the inlet and outlet, °C	q	volumetric heat source, W/m^3
T_{pc}	Phase change temperature, °C	α	Coefficient of thermal expansion，1/°C
ΔT	ΔT= T$_{in}$- T$_{out}$, °C	λ	Thermal conductivity, W/(m·K)
$\overline{\Delta T}$	Average temperature difference	δ	Thickness, mm
P	Pressure, Pa	R	Thermal resistance, °C/W
c_p	Specific heat, kJ /(kg·K)		Abbreviation
q	Volumetric heat source, W/m^3	IAT	Inlet air temperature
t	Time, s	ASV	Air supply velocity
f	Liquid fraction	PCT	Phase change temperature
L, W, H	Length, Width and Height	PCES	Phase change energy storage
W_r	Anterior-to-posterior slope ratio of PCP	PCM	Phase change material
L_f	Length of fin	PCP	Phase change plate
V_a	Inlet air velocity, m/s	V	Value coefficient
	Greeks	F	Function coefficient
ρ	Density, Kg/m^3	C	Cost factor
μ	Dynamic coefficient of viscosity，N·s/m^2		

1. Introduction

Data centers, as information processing carriers, contribute mightily to the vitality of businesses in the digital economy [1,2]. However, the normal operation of data centers requires a huge amount of energy, with their electricity consumption accounting for about 1% to 1.5% of the global electricity consumption [3,4]. The total energy consumption of data centers in China was 266.792 billion kWh in 2023, exceeding the total electricity consumption of Australia in 2018 [5]. The air conditioning system is an important subsystem of the data center, which maintains the temperature and humidity inside the server room within the normal operating environment requirements of IT equipment [6,7]. The cooling system accounts for about 40% of the total electricity consumption of the data center being the largest energy consumption except IT equipment [8,9]. Although traditional cooling methods such as mechanical refrigeration and liquid cooling can meet the cooling requirements [10], they suffer from high electricity consumption, high water consumption and environmental impact [11,12]. Therefore, it is urgent to find energy-efficient, high-efficiency and environmentally friendly cooling technologies for data centers.

Free cooling technology provides the cold source for server room by utilizing natural cold air for heat exchange and is a key focus of the data centers industry [13,14]. As the goal of carbon peak and carbon neutrality is established [15], the use of free cooling for refrigeration is the basic way to achieve zero carbon emissions in cooling systems [16]. Li et al. [17] utilized cold mist direct evaporative cooling technology with natural cold sources to cool high-temperature fresh air, significantly reducing carbon emissions from data centers. Fan et al. [18] designed a novel free cooling system that can reduce refrigeration energy consumption by 4.4%~62.6% in different regions. Temiz et al. [19] designed a renewable energy power generation system for data center refrigeration, which reached 24.33% of the energy conversion taking advantage of the environment of the Arctic. Wang et al. [20] confirmed that the application of direct free cooling for data center refrigeration is technically and economically feasible to a certain extent.

Phase change energy storage (PCES) utilizes phase change material (PCM) to absorb or release large amounts of latent heat during phase change for energy storage [21] and temperature regulation [22,23]. Bin et al. [24] designed a novel PCES system, achieving the emergency refrigeration for 300s under the conditions of an inlet temperature range of 31°C to 39°C. Priyadarshi et al. [25] proposed that paraffin-bonded desiccants for cooling systems could save energy and improve air quality. Ren et al. [26] proposed a heat exchanger with multiple ring-shaped PCM layer conduits to increase the fresh air treatment capacity. Wang et al. [27] mixed liquid metal with PCM for CPU cooling resulted in 23% energy conservation. Yi et al. [28] found that the use of PCP enabled the free cooling capacity to be continuously released into the server room during the high-temperature period. Yang et al. [29] proposed a PCP-assisted direct ventilation natural cooling system for data center cooling, which could reduce the 70% energy consumption. Combining free cooling with PCES for cooling systems facilitates to transformation of their energy structure towards energy conservation and environmental protection [30,31]. However, the application of PCES in data centers still faces challenges, especially how to optimize the structure of PCP, making PCMs evenly heated and improve energy storage efficiency and thermal performance.

The thermal performance of PCM can be enhanced by using different container geometries such as spheres, squares, trapezoids and triangles [32]. Liang et al. [33] evaluated the thermal performance of PCP in different configurations through case studies of data centers to enhance grid stability and reduce costs. Zhu et al. [34] numerically studied latent heat storage of PCM with different fin configurations to optimize the working strategy. Kosdere et al. [35] studied the influence of different fin geometry parameters on heat transfer coefficients and developed a lower-cost radiator. Boujelbene et al. [36] found that channel geometry was considered as an effective technique to enhance the melting/solidification performance of PCM. Poorya et al. [37] found that PCP melting time with a stepped fin structure was reduced by 52% compared with a straight fin structure under the same conditions. Najim et al. [38] numerical investigated the effects of adding a new design fins arrangement to a latent heat storage system, revealing that utilizing the tringle fins enhances the thermal performance. Guo et al. [39] found that a high-humidity environment can greatly increase the melting rate of PCP under experimental conditions by more than 60%. Ma et al. [40] found that the cooling ability increased with the increase of PCM thermal conductivity through experiments and numerical simulation. Most designs of PCP mainly rely on conventional planar or sheet structures now [41,42]. Although these structures have advantages in cost [43,44], they have certain limitations in heat transfer efficiency and energy storage capacity [45]. Geng et al. [46] deemed that PCM face limitations in terms of regulating phase change temperature, low thermal conductivity and so on.

In conclusion, although the integration of free cooling with PCES enhances energy conservation of data center cooling systems, rectangular cavity PCP exhibits uneven melting due to structural limitations. However, the conventional PCP often exhibits non-uniform melting, which negatively affects the overall performance of the system. Therefore, achieving uniform heating of the PCP to enhance heat transfer efficiency and promote energy conservation is a critical challenge in the optimization of cooling performance.

This research aims to improve the effectiveness of PCP-assisted free cooling for the data center located in Gui'an New District, Guiyang, Guizhou Province, China. A novel scheme based on the optimization of a uniformly heated PCP structure is proposed in this paper. Specifically, firstly, compared the different anterior-to-posterior slope ratios to make the PCP melt evenly. Secondly, double fins are incorporated into PCP to further improve its thermal performance, and the optimal configurations of these fins are examined. Finally, the economical and suitable volume of PCP is determined in combination with PCP's charging and discharge requirements. Additionally, the effects of different inlet air temperatures (IAT), air supply velocities (ASV), phase change temperatures (PCT) and thermal conductivities (λ) are studied to analyze the relationship between the system cooling performance and them. This study promotes the evolution of data center industry in a green and low-carbon direction.

2. Methodology

2.1 Experimental principle

Compared the trends of the ambient temperature and the power load in the server room during the high temperature in summer to explain the experimental principle, as shown in Fig.1 (a). The outdoor air temperature and the power load in summer have similar change trends, and the time points at which they reach the minimum and maximum values are relatively close to each other. Before 9:00 a.m., the outdoor air temperature does not exceed 27°C, and the power consumption of the server room is in the off-peak period. After 9:00 a.m., the outdoor air temperature gradually increases, reaching approximately 34°C between 12:00 p.m. and 3:00 p.m., during which time the power consumption of the server room peaks.

The combined application of natural cold air and PCES mainly contains two processes. The first process is the charging process of PCP. During the off-peak h of the server room, the outdoor cold air can be directly passed into the server room for cooling after a little treatment. And the load of the server room is minimal, resulting in the underutilization of the cold air. The PCP stores the nature cold air at night. The second process is the discharge process of PCP. The PCP that has been solidified by cold air is in contact with high-temperature air for heat exchange. The PCM absorbs heat and gradually undergoes melting, resulting in a progressive cooling of the air.

The natural cold air at night solidifies the PCM and completes the charging of the PCPs. The working principle of the daytime system is shown in Fig.1 (b). The outdoor high-temperature air and little hot air generated by the server enter the front end of the channel, exchanging heat with the concretionary PCPs at low temperatures. The treated cold air is sent into the air intake area passage of the racks by the fans. Then cold air cools down the servers that are running at high temperatures.

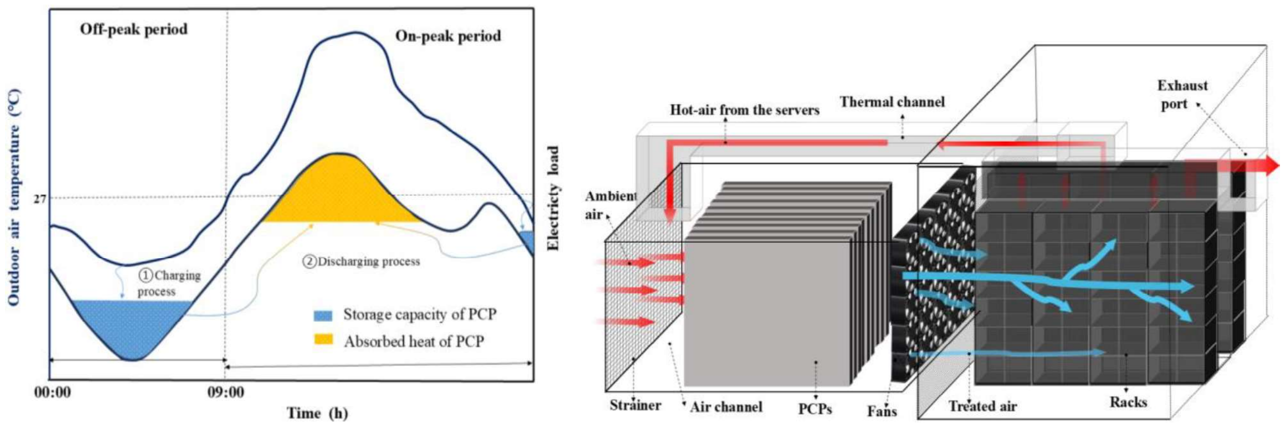

(a) Research technical schematics (b) System working principle

Fig .1. Experimental principle

2.2 Experimental details

The experimental platform of PCP-assisted free cooling is shown in Fig.2. The experimental platform is mainly composed of three parts: the artificial environment room, the combined system and the data acquisition instrument. The artificial environment room is consisted of three parts: the console platform, the ventilation room and the cooling room. It controlled the air temperature in the environmental laboratory at -20°C~50°C, and the control accuracy did not exceed ± 0.5°C. The direct ventilation channel was assembled from 5mm thick acrylic sheet lap joints, with dimensions of 200cm

(L) ×70cm (W) ×65cm (H). PCPs were placed at 45 cm away from the inlet end in the channel. These PCPs with dimensions of 100 cm (L) × 3 cm (W) × 58 cm (H) were welded into a rectangular cavity using 1 mm thick stainless steel sheets. A total of 10 PCPs were evenly placed in the channel, with the distance of 4 cm between each two. Four PT100 thermocouple wires were evenly inserted inside each PCP to capture the temperature changes as the PCM melts and solidifies. Paraffin wax was encapsulated inside the PCPs. The main thermal performance parameters of the experimental material paraffin are shown in Table 1.

(a) all (b) top

(c) inside (d) back

Fig .2. Details of the experimental platform

Table 1

PCM thermal performance parameters

Paraments	**Values**
Material	Paraffin wax
Phase change temperature (℃)	25. 84
Density (kg/m³)	880 - 770 (solid-liquid)
Thermal conductivity (W/(m·K))	0.21
Latent heat (kJ /kg)	217
Specific heat (kJ /(kg·K))	3.22
Flashing point (℃)	> 250
Maximum working point (℃)	200
Pure solvent melting heat (J/kg)	165900

2.3 Working condition design

The control variable method and the interpolation method were used to design the simulation conditions. Firstly, the W_r was studied for the uniform melting of PCM. Secondly, to further enhance the thermal performance of PCP and improve structural stability, the optimal position of the double-fin layout in PCP was explored. Then, to facilitate the practical application of the PCP with an optimized structure and configuration, the external environment and the thermal parameters of PCM were studied.

2.3.1 Optimization of the anterior-to-posterior slope ratio of PCP

The discharging experiment of PCP in the system was carried out in the early stage of the design. It was found that at the end of the experiment, the front part of PCP was almost melted, while there was some solid PCM in the partial back end, as shown in Fig .3 (a). Because the front end of the PCP is preferentially exposed to high-temperature air, so the front end of the PCM is preferentially melted over the back end. In this paper, the width of the front end of the PCP (W_1) was gradually increased and the width of the back end of the PCP (W2) was reduced under the premise of controlling the total capacity of PCM and the length and height of the PCP were consistent with the experimental research, as shown in Fig .3 (b). Interpolation method was used in this study. At first, the optimization range was gradually narrowed through extensive W_r comparisons. Finally, the feasible range was defined as 1~2, and four groups of optimization proportions were gradually refined, as shown in Table 2.

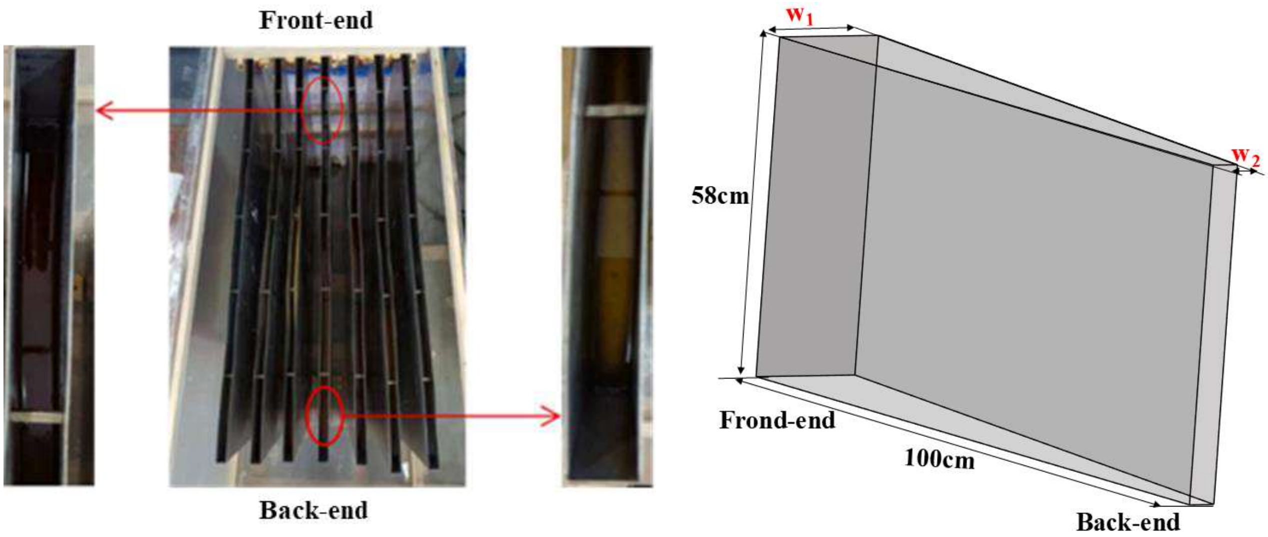

(a) Uneven melting of rectangular PCP (b) Structure size of trapezoidal PCP

Fig .3. W_r design of PCP

Table 2

Different parameters of W_r

Model	W_1 (cm)	W_2 (cm)	W_r（W_1:W_2）
Experiment	3	3	1
1	3.33	2.67	1.25
2	3.6	2.4	1. 5
3	3.815	2.185	1.75
4	4	2	2

2.3.2 Double fin layout design

The double fin can provide enough surface area to accelerate the heat transfer and is more uniform and stable than the single fin [47]. Compared with multiple fins, double fins are structurally simpler, avoiding the potential for complex flow patterns and additional weight to affect overall efficiency [48,49]. In this study, the layout design of the double fins is studied as shown in Fig .4. Both sides of these three layouts are arranged close to the inner wall of the PCP, and the fins are 50cm long and 0.1cm thick.

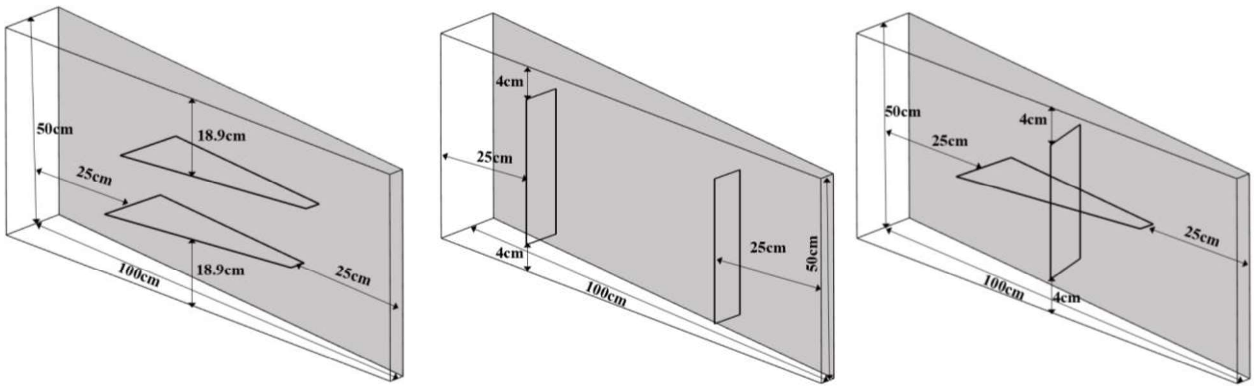

(a) (b) (c)

Fig .4. Layout diagram of the fin of the inner PCP: (a) Vertical parallel-A; (b) Horizontal parallel-B; (c) Cross parallel-C

2.3.3 Simulation conditions

The temperature in the server room is required to be between 18°C and 27°C, and the highest temperature record in Gui'an in the past three years is 34.4°C, so the temperature range explored is 28°C-36°C. The ASV of the direct ventilation system is calculated concerning the scale of the data center in the Gui'an. The size of the machine room is 18m (L) ×16m (W) ×6m (H), and the required air volume is 1968m^3/h~4076m^3/h, that is, ASV is 1.21m/s~3.47m/s.

A total of 19 sets of cases are involved in this study, as shown in Table 3. Cases 1 and 2 are used for computational preparation, case 2 is used in the optimization part of the PCP unit, and additional cases are added for sensitivity analysis.

Table 3

The simulation conditions

Case	T_{in} (°C)	V_a (m/s)	T_{pc} (°C)	λ (W/(m·K))
1	32	3	25. 84	0.21
2	30	2	25. 84	0.21
3	28	2	25. 84	0.21
4	32	2	25. 84	0.21
5	34	2	25. 84	0.21
6	36	2	25. 84	0.21
7	30	1.5	25. 84	0.21
8	30	2.5	25. 84	0.21
9	30	3.0	25. 84	0.21
10	30	3.5	25. 84	0.21
11	30	2	23	0.21
12	30	2	24	0.21
13	30	2	25	0.21
14	30	2	26	0.21
15	30	2	27	0.21
16	30	2	25. 84	0.11
17	30	2	25. 84	0.31
18	30	2	25. 84	0.41
19	30	2	25. 84	0.51

2.4 Numerical model

The *k-e* model was used to solve the calculation model to visualize the changes in the interface during the solidification and melting of PCM. The Standard *k-e* model was adopted as a turbulence model for the calculation of natural convection heat transfer problems [50]. Necessary assumptions are made to the numerical model to simplify the calculation [51,52]:

(1) Both air and PCM in the calculation domain are isotropic;

(2) Air is Newton incompressible;

(3) Each air channel in the system is evenly arranged, assuming that the ASV of the heat transfer fluid is uniform;

(4) Heat transfer is mainly through convection and heat conduction, ignoring radiant heat

Transfer;

(5) The air wall is a constant temperature boundary;

(6) Ignore the viscous effects of the fluid.

Based on the above Settings, the following governing equation can be used to calculate.

Continuity equation:

$$\frac{\partial \rho}{\partial t} + \nabla . \rho v = 0 \tag{1}$$

ρ is the paraffin density (kg/m^3), t represents time (s), and v represents the velocity vector (m/s)

Momentum equation:

$$\rho \frac{\partial v}{\partial t} + \rho \mathbf{u} . \nabla v = -\nabla p + \mu \cdot \nabla^2 v + \rho \alpha (T - T_{ref}) g + S \tag{2}$$

Where ρ is the pressure (Pa), μ is the dynamic viscosity coefficient (N·s/m^2), α is the coefficient of thermal expansion (1/K), T_{ref} is the temperature value of the reference surface, g is the gravity (m/s^2), and S is the source term of the momentum equation, which can be calculated as follows:

$$S = \frac{(1+f)^2}{(f^3+\omega)} A_{\mathrm{mush}} v \tag{3}$$

f is the liquid fraction, ω is the coefficient to avoid zero division taking 0.001, and the continuity coefficient of amush solid-liquid mixing takes 1×10^5. The formula for calculating f is as follows:

$$f = \begin{cases} 0 & T_{pcm} \leq T_s \\ \frac{T_{pcm} - T_s}{T_l - T_s} & T_s < T_{pcm} < T_l \\ 1 & T_{pcm} \geq T_l \end{cases} \tag{4}$$

Where T_{pcm} is the temperature of PCM at any time (°C), T_s is the temperature at which PCM begins to melt (°C), and T_l is the temperature at which the melt ends (°C).

Energy equation:

$$\boldsymbol{\rho c_p\left(\frac{\partial T}{\partial t}+v.\nabla \mathrm{T}\right)=\lambda\nabla^2 T+q} \tag{5}$$

Where c_p is specific heat (kJ/(kg·K)), λ is thermal conductivity (W/(m·K)), q is volumetric heat source (W/m^3).

2.5 Solution methodology and numerical validation

Based on the experimental setup of the previous study, a numerical computational model of the PCP direct venting unit of the same specification was built using ANSYS ICEM 2022. The physical model dimension of the ventilation system was 200cm (L) ×70cm (W) ×65cm (H). 10 PCPs were evenly distributed in the center within the model.

Numerical simulations were carried out using ANSYS Fluent 2022. The computational region was set as an unsteady, laminar/turbulent, solid/liquid phase change model. The inlet was set as pressure inlet boundary condition, the outlet was set as free flow outlet boundary condition, the outer wall of the channel was the heat flux. And walls between PCP and fin were set as coupled. According to experimental results and meteorological data of Gui 'an, for charging progress, the initial temperature of PCM was 26.5°C. For discharging progress, the initial temperature of PCM was 22°C.The gravity was 9.8 m/s^2 and the operating pressure was 101325 Pa.

The SIMPLE algorithm was used for transient calculations and a second-order formulation was used to ensure numerical accuracy. The relaxation factors for Pressure, Momentum, Turbulent Kinetic Energy, Turbulent Dissipation Rate and Turbulent Viscosity were set as 0.7, 0.3, 0.5, 0.8 and 1. The simulations converge when the residuals of both mass and momentum were less than 1×10^{-3} and the residuals of energy were less than 1×10^{-6}.

2.5.1 Grid independence

The numerical computational model is a standard symmetric structure. A structural mesh was used to divide the numerical computational model into two basins, one for the air basin and the other for the PCM solid-liquid mixing. The schematic diagram of the grid division of the calculation area is shown in Fig.5.

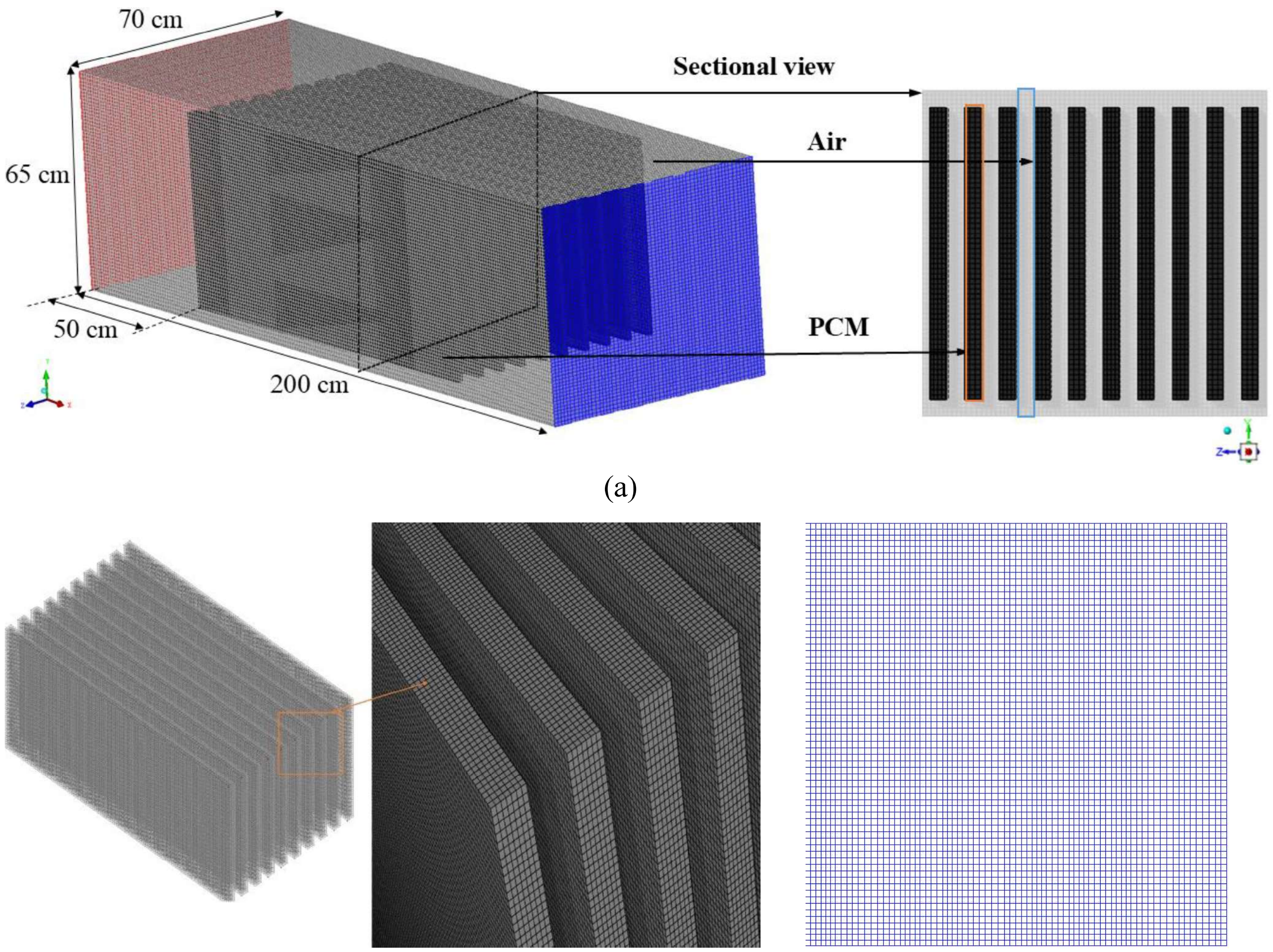

(a)

(b) (c)

Fig .5. Model grid. (a) Grids of the system; (b) Grids of the PCM; (c) Grids of the outlet

To ensure that the numerical simulation results are not affected by the computational grid density, five different structured grids were divided for grid independence verification. All the grid qualities are 1, and their numbers are 586332, 834987, 989874, 1215028, and 1779456.

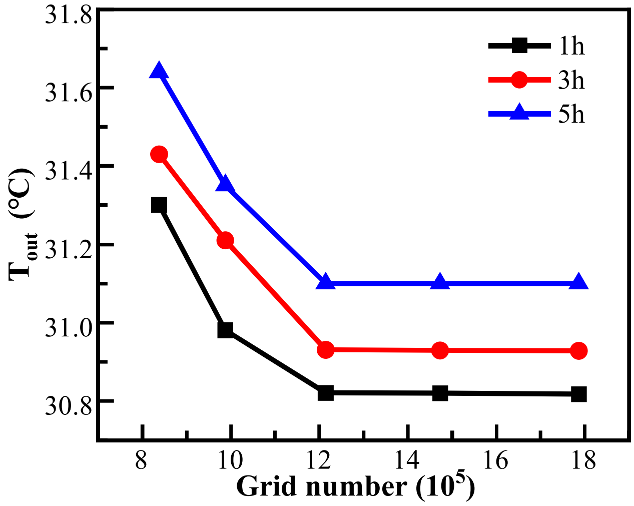

Fig .6. Number of grids

Fig.6 plots the trend of T_{out} at 1h, 3hand 5h with the increase of the number of grids. Compared with that of higher than 12×10^5, the T_{out} at different moments is larger when the number of grids is lower than 12×10^5. After 12×10^5, the T_{out} remains almost unchanged as continues to generate finer grids for the computation. The number of grids was chosen to be about 12×10^5 for economical and appropriate computational accuracy.

2.5.2 Time step

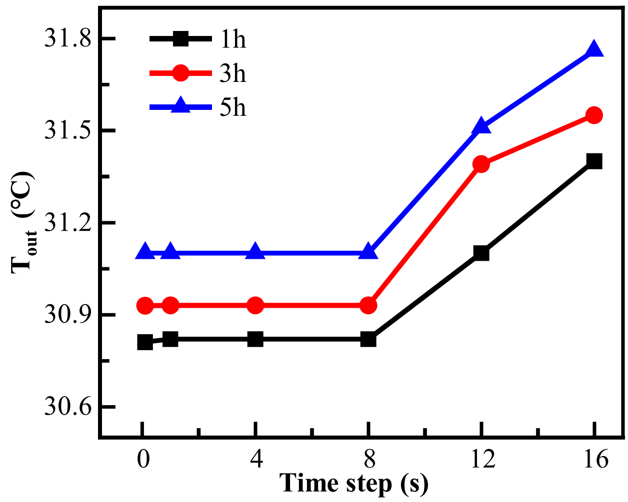

Fig .7. Time step

At the beginning of the computation, a small-time step of 0.1s was used to increase the convergence rate. As the computation converges, gradually increase the time step to reduce the computation time. As shown in Fig.7, it can be noticed that when the time step is less than 8s, the time step has little effect on the computational results. But when the time step is greater than 8s, the computational results change significantly with its increase. Therefore, the numerical results fluctuate within an acceptable range for 8s. In the following numerical simulation, the time step is set to 8s.

2.6 Model validation

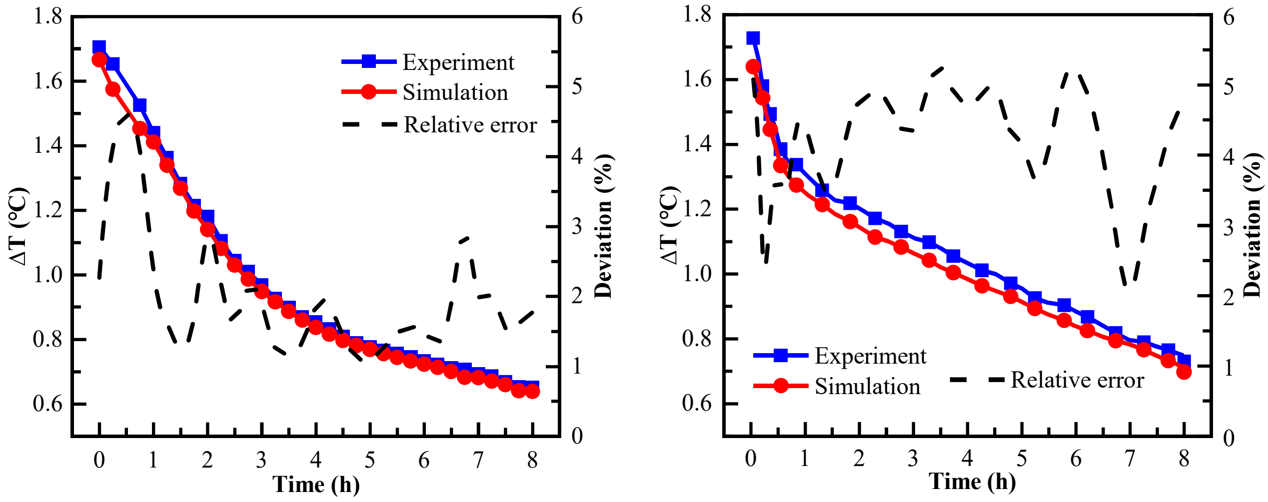

(a) T_{in} = 30°C, V_a = 2m/s (b) T_{in} = 32°C, V_a = 3m/s

Fig .8. Model validation

Two different operational conditions were selected to validate that the model can accurately predict the heat exchange process between PCPs and air. Fig .8 compares the temperature difference between the inlet and outlet (ΔT) of the system during the experiment and simulation respectively. From Fig .8 (a) and Fig .8 (b) can be seen that the simulation shows the same downward trend as the experiment curve, and numerical simulation results are slightly less than experimental results. As in the experimental process, the ventilation device built in the experiment has a few gaps for heat dissipation, but the wall of the device in the simulation is set to be insulated. The deviation value is expressed as the absolute value of the difference between the experimental value and the simulated value, divided by the percentage of the experimental value. The deviation of the two conditions is all less than 10%. And the maximum deviation value is 5.3%. Considering the existence of certain fluctuations in the experimental conditions, the error in the model validation is within the acceptable range, and the model is reliable and can be applied in subsequent research.

3. Results

3.1 Thermal performance of the PCP

3.1.1 Charging process

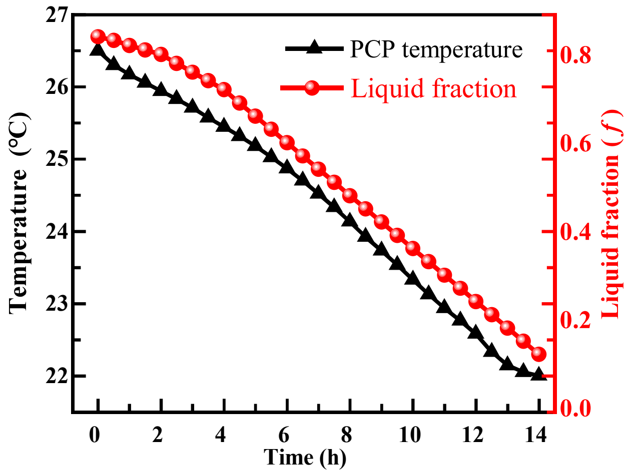

Fig .9. Thermal parameter curves in the PCP charging process

The charging process of PCP is studied by using the rectangular PCP model when the T_{in} is 22°C and the ASV is 2m/s is simulated. The PCP temperature and the liquid fraction of PCM (*f*) during the charging process are plotted in Fig.9. Both the PCP temperature and the *f* show a decreasing trend with the increase of time. At the beginning of the cold storage simulation, the PCP temperature at which discharge is completed during the day is around 26.5°C. As the natural cold air is continuously delivered into the direct ventilation channel, the high-temperature PCP encounters the cold air for heat exchange, so the temperature is reduced. After nearly 14 h, the PCP temperature drop intersects with the inlet temperature and tends to coincide, indicating that the night charging is complete. The *f* reaches 0.15. Under this condition, it takes about 14 h to complete the PCP charging.

3.1.2 Discharging progress

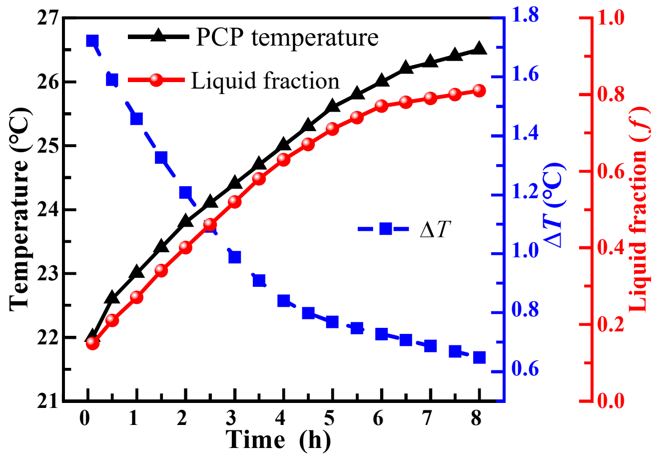

Fig .10. Thermal parameter change curve in PCP discharging process

Fig .10 plots the change of PCP temperature, ΔT and f when the IAT is 30°C and the ASV is 2 m/s. The PCP temperature and the f show the trend of increasing rapidly first and then slowly with the increase of time. The ΔT drops rapidly first and then drops slowly with the increase of time. When the PCP temperature rises near the PCT (25. 84°C), the change of the PCP temperature is relatively small. The value of f increases from 0.15 to 0.81, which means 81% of the PCM has melted, and 19% remains solid. 15% liquid paraffin wax means that some latent heat still has not been released. Incomplete solidification will reduce the total cold storage capacity of the system and may not meet the continuous cooling requirements. However, a temperature drop of 1.5°C within the first hour can be regarded as effective cooling. In the first 2h, the ΔT shows a sharp decreasing trend. After that, the ΔT slowly decreases with time and finally stabilizes. The cooling range of PCPs is 0.6 -1.7°C, and the total heat capacity of PCPs is 5534 kJ under this condition.

3.2 Optimization of the PCP unit

3.2.1 Anterior-to-posterior slope ratio of PCP

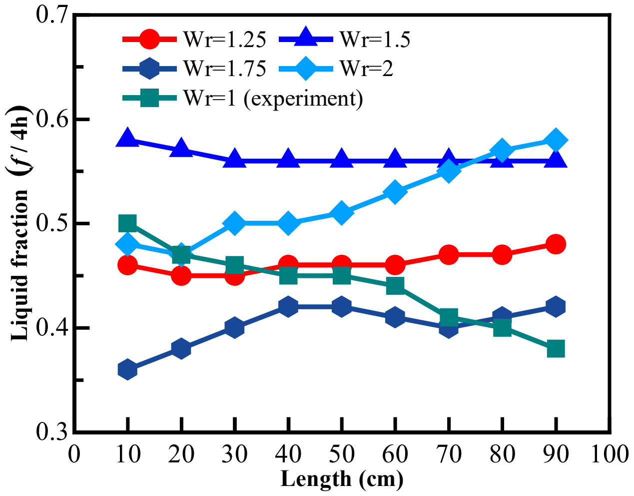

(a) The variation of liquid fraction found along the length of PCP at 4 h

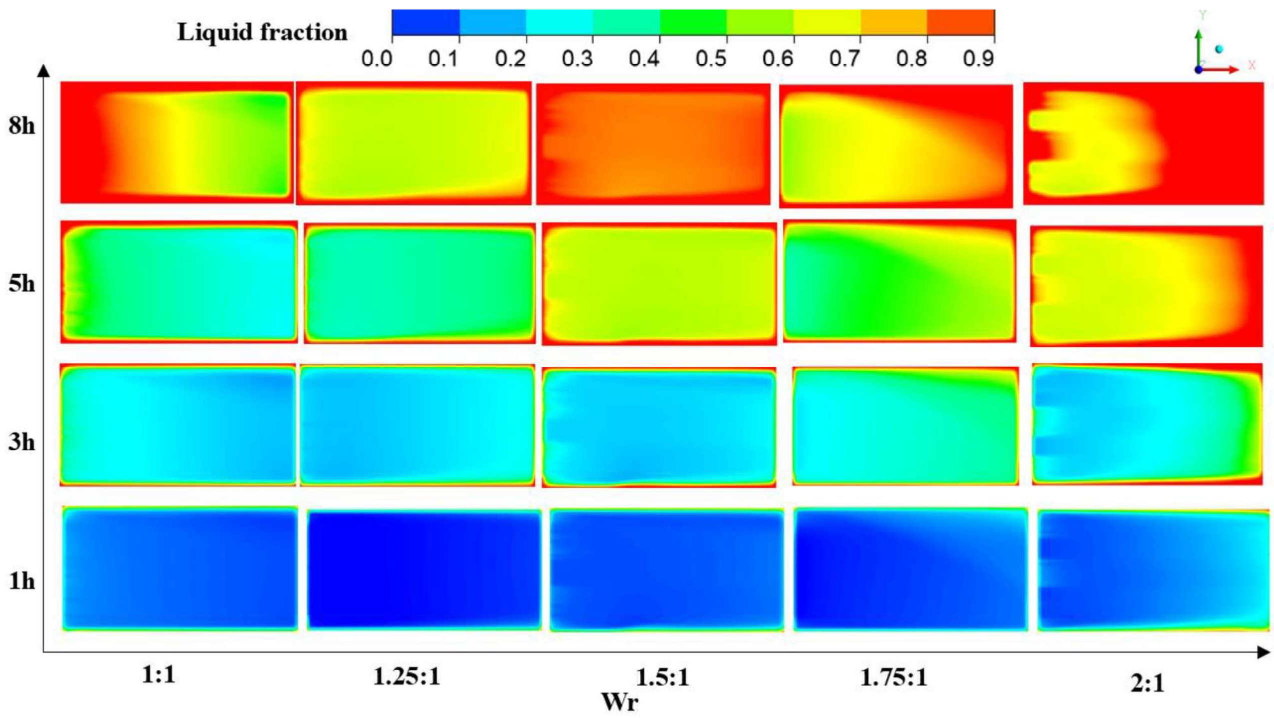

(b) Liquid cloud map at the central cross-section of PCP

Fig .11. The influence of different W_r on the uniformity

The f is used as the index to assess the uniformity melting of PCP. Specifically, the values of the f at monitoring points set at intervals of 10 cm along the length direction of the PCP are selected for analysis. Compared these values after a duration of 4 h with the IAT is 30°C and the ASV is 2.0 m/s.

From Fig. 11 (a) can be observed that when W_r is 1, the f at the front end of the PCP reaches 0.5, while at the back end it is 0.4. When W_r is set to 1.25 and 1.5, the f of different locations remains stable. In comparison, the f at W_r of 1.5 is both more stable and higher. When the W_r is 1, 1.25, 1.5, 1.75 and 2, the variances of the f at different measurement points are 1.4×10^{-3}, 9.4×10^{-5}, 5×10^{-5}, 4.2×10^{-4} and 1.5×10^{-3} respectively. The smaller the variance indicates that the f at each point is closer to the average value, and the PCP melting is to closer uniformity. So, selecting a W_r of 1.5 results in a 93% enhancement in the uniformity of melting at both the front and back ends of the PCP.

Compared the liquid cloud maps of the central cross-section of PCP of five different W_r to study the effect of the W_r on the melting uniformity of PCM, as shown in Fig.11 (b). The PCP with a W_r of 1 has a larger front-end f during the simulation. The PCPs with a W_r of 1.75 and 2 both have a larger back-end f. The PCP with W_r of 1.25 and 1.5 has similar f in the front-end and posterior parts. For uniform melting of PCM can be judged that the PCP with a W_r of 1.25 and 1.5 is a feasible board optimization ratio.

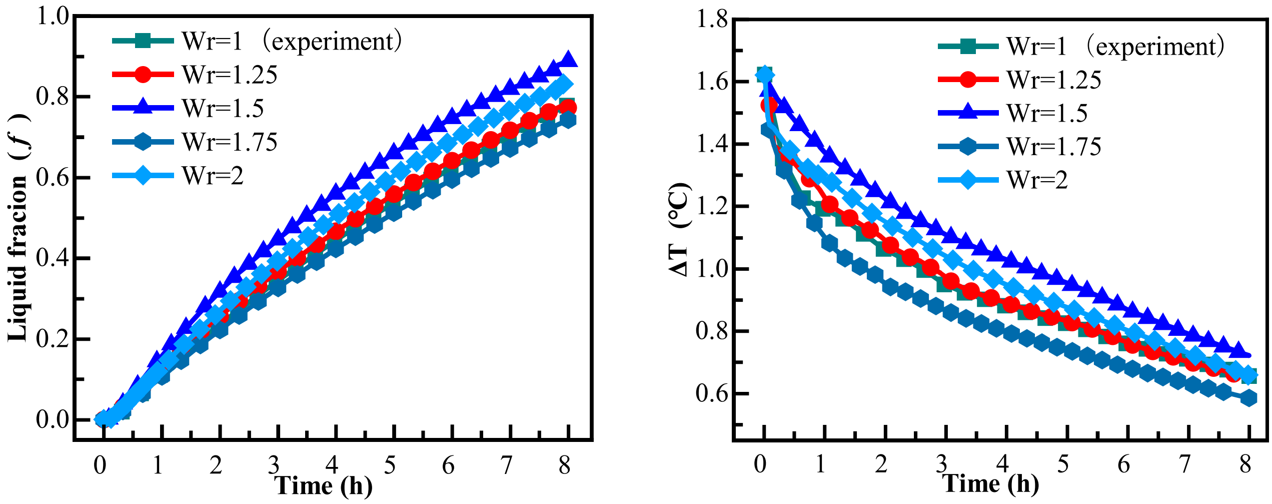

(a) (b)

Fig .12. The influence of different W_r on the system: (a) Liquid fraction; (b) Temperature difference between inlet and outlet

Fig.12 (a) compares the trend of the f at the time of PCM melting with different W_r. The f

gradually increases with time. The f is higher when W_r is 1.25, 2and 1.5 than those of the initial experimental setup. The W_r is 1.5, which is the highest overall. When W_r changes from 1 to 1.5, the f reaches 0.89, increasing by 11.1%. The f of the 1.75 W_r is lower than that of the experimental setup, which is the smallest among the five ratios.

Fig.12 (b) compares the effects of different W_r on the ΔT. The ΔT shows a gradual nonlinear low trend with time. The W_r of 1.25 is analogous to that of the experimental device (the W_r is 1). The ΔT of the PCP system with a W_r of 1.75 is lower than the experimental device, which is the smallest among the five W_r. The ΔT with a W_r of 1.5 and 2 is higher than that of the initial experimental setup. When the W_r is 1.5, the ΔT is the highest among the five ratios, ranging from 1.6°C to 0.8°C.

From discussion above can be concluded that the overall thermal performance of the system is better when the W_r is 1.5. Therefore, the optimized W_r of the PCP of the system is 1.5.

3.2.2 Double fins layout

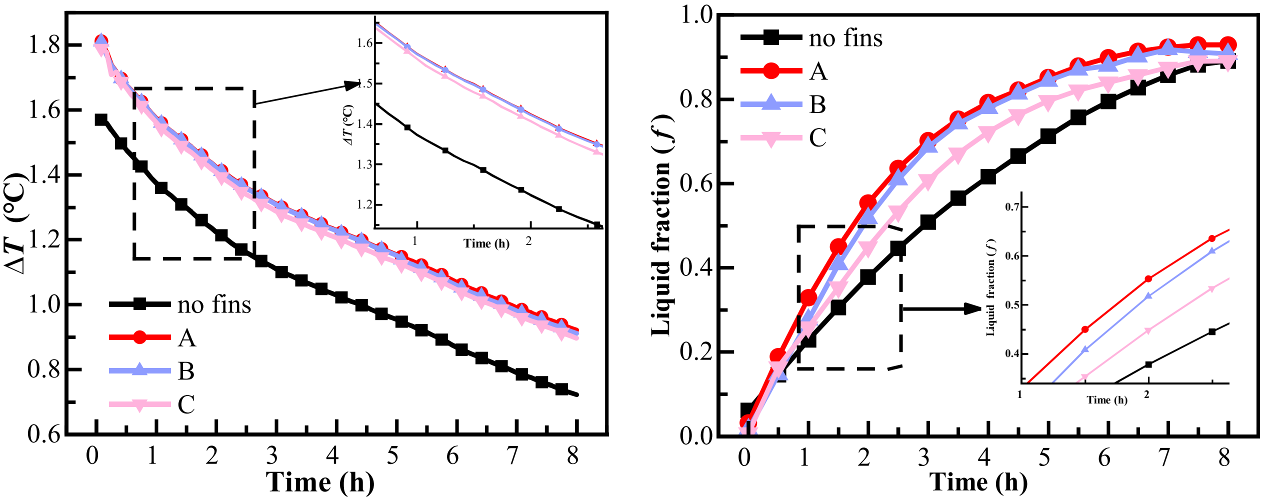

(a) ΔT (b) Liquid fraction

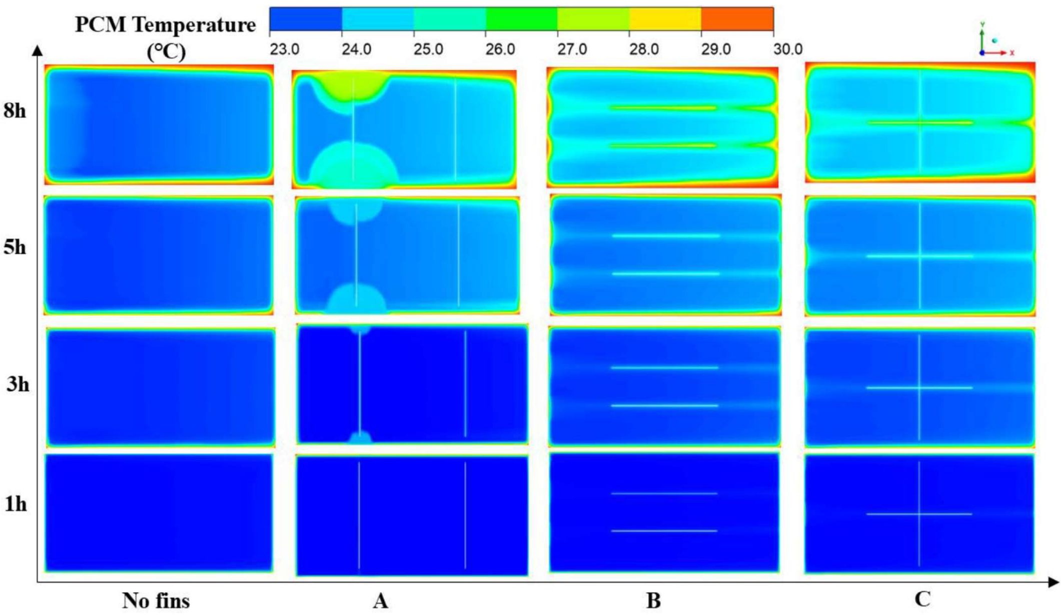

(c) Temperature cloud image at the central cross-section of PCP

Fig .13. The effect of adding fins at different locations on system performance

Fig.13 compares the effect of adding fins at different locations within the PCP. Fig.13 (a) shows the ΔT over time with different double-fin layouts. The ΔT of PCP with fins is significantly greater than that of no fins. The addition of fins in the PCP indirectly increases the contact area between the hot air and the PCM, which improves the cooling performance of the system by about 14%.

The variation curve of the f gradually increases with time, and the f with fins is significantly larger than that of no fins, as shown in Fig.13 (b). However, the ΔT curves and the f trends and values of the three different fin layouts are consistent. The ΔT caused by these three is 0.01 °C~0.24 °C, and the temperature difference of the f is 0.03~0.07. According to the enlarged image, A and B are slightly better than C.

In addition, from Fig.13 (c) can also be seen that the fin layout has a certain degree of influence on the system. After 3 h, the PCM temperature around the fin is slightly higher than that at other parts. Compared A with B, the B makes the overall temperature distribution of PCP more uniform. In summary, B is chosen as the preferred fin layout.

3.2.3 The volume of PCP

The volume is adjusted by factors of 0.4 and 0.8, respectively, to modify the volume relative to the original 19 L. When PCM temperature drops to 22°C, charging is considered complete, and the time it takes is the charging time. The time when the ΔT is greater than or equal to 1°C during the melting process is regarded as the effective discharging time.

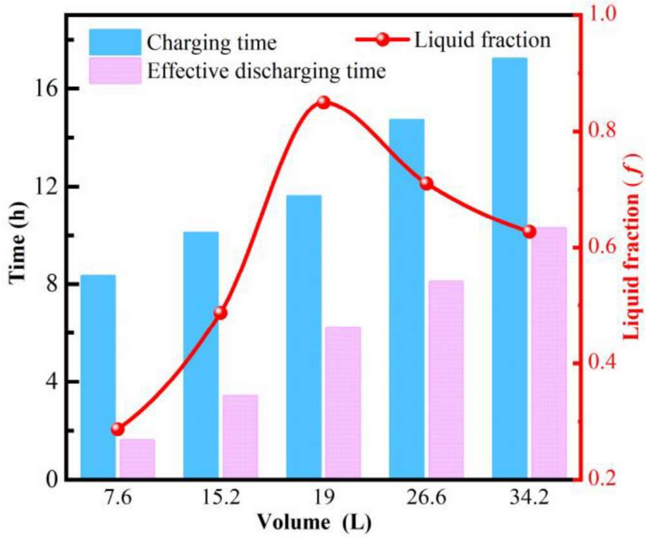

Fig .14. Effect of volume on solidification time, effective working time and liquid fraction

From the Fig.14 can be seen that the solidified time and effective working time of PCP are extended with the increase of volume. In addition, the liquid fraction at the time of losing cooling abilities increases first and then decreases with the increase of volume. And the liquid fraction reaches peak of 0.85 when PCP volume is 19 L. The volume reduces to 0.4 times the original (7.6 L) needs 8.3h to charge and works effectively for 1.6h, and the liquid fraction is 0.29. The charging time and discharging time increase by 3.3 h and 4.6 h respectively and the liquid fraction increases by 0.56 when the volume increases from 7.6 L to 19 L. Compared with the 19 L and 26.2 L, the volume is increased by 1.4 times, the charging time increases by 3.1 h, the effective working time increases by 1.8h, and the liquid fraction decreases by 0.12.

Considering that the cold storage time at night is limited and does not exceed 14 h, the applicable volume does not exceed 26.6 L. According to statistics, the temperature on a high-temperature day usually lasts for about 4 h, and the effective working h should exceed 4 h. It should exceed 15.2 L. Therefore, the suitable volume range for PCP is between 15.2 L and 26.6 L. Therefore, the suitable and cost-effective capacity within the system is 19 L. The more the volume of the PCP increases, the charging time and PCM will also increase. Based on the necessity of fulfilling the cooling requirements of the data center, a smaller size of the PCP will lead a reduction in operating costs. The f reaches the maximum value within the appropriate range when the volume is 19 L. Its performance is cost-effective. The charging time of the optimized system is 11.6 h, which is 28% shorter than that of the rectangular PCP of the same volume.

3.3 Sensitive analysis

3.3.1 Effect of the inlet air temperature

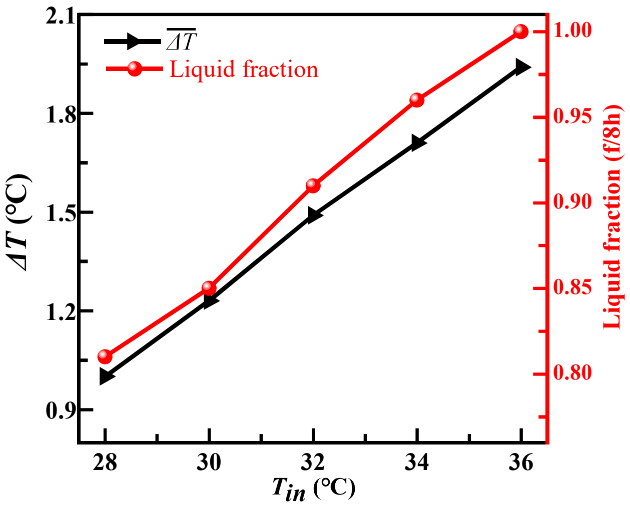

Fig .15. The influence curve of IAT

Fig .15 compares the 8-hour average temperature drop ($\overline{\Delta T}$) and final liquid fraction trend of the system at PCT of 25.84°C, λ of 0.21, ASV of 2m/s, and IAT of 28°C, 30°C, 32°C, 34°C and 36°C. It can be observed that the $\overline{\Delta T}$ and liquid fraction of the system show an approximately linear upward trend with the increase in IAT. This simulation study satisfies the general theorem that the larger the temperature difference, the stronger the heat transfer. The greater the difference between the temperature of the heat exchange fluid and the melting point of the PCM, the stronger the driving force for heat transfer becomes. Therefore, more heat is transferred per unit time, resulting in a greater final degree of melting.

When the IAT is 28°C, the system is cooled by an average of 0.96°C within 8 h, and the PCP melted by 81%. The system almost meets the supply air temperature requirements of the data center at 28°C. When the IAT increases from 28°C to 34°C, the system cooling increases by about 0.8°C, and the liquid fraction increases by 0.15. The average increase in cooling capacity is approximately 89% from 28°C to 34°C. At the IAT of 36°C, the $\overline{\Delta T}$ and liquid fraction is the largest, and the average PCP per meter is cooled by about 1.95°C. It is more than twice that at 28°C. When the inlet temperature significantly exceeds the phase transition temperature, the surface of the paraffin may rapidly melt, resulting in the formation of a liquid layer. Should a temperature differential exist between the liquid paraffin and the heat exchange fluid, this will facilitate enhanced internal heat transfer. Conversely, if the inlet temperature approaches the phase transition temperature, the melting process occurs at a slower rate and predominantly depends on heat conduction.

3.3.2 Effect of the inlet air velocity

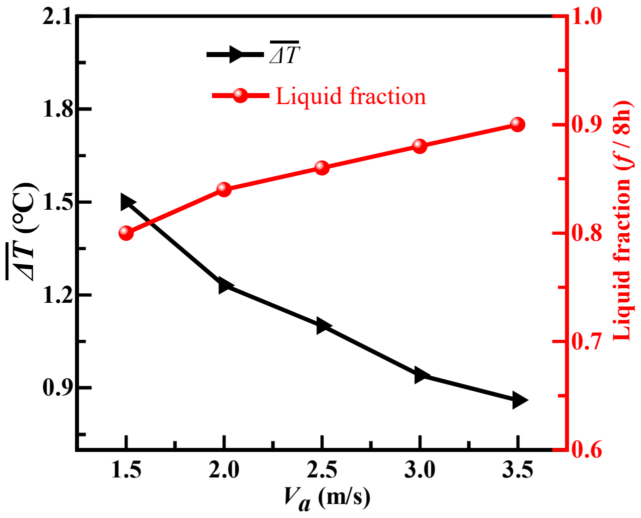

Fig .16. The influence curve of ASV

Fig .16 compares the $\overline{\Delta T}$ and the final liquid fraction trend of the system within 8 h when the IAT is 30°C and ASV is 1.5 m/s, 2.0 m/s, 2.5 m/s, 3.0 m/sand 3.5 m/s, respectively. The $\overline{\Delta T}$ decreases with the increase of ASV, but the liquid fraction increases with the increase of ASV. The rapid velocity of ASV results a short heat exchange duration between the PCM and the hot air, preventing the PCM from fully releasing its heat. But higher ASV can provide more heat to PCP, which makes PCM melt faster and the liquid fraction grows faster. Because the ASV increases, the boundary layer between the fluid and the surface of the PCP becomes thinner, resulting in reduced thermal resistance. So, heat is transferred more efficiently to the surface of the PCP.

When the ASV is 1.5m/s, the $\overline{\Delta T}$ of the system is 1.5°C, and the liquid fraction is 0.8. When the minimum ASV increases to 2.0 m/s and 2.5 m/s, the temperature drop difference between adjacent wind speeds varies greatly. The liquid fraction just increases by 0.02 but $\overline{\Delta T}$ decreases by 14% when the ASV increases from 2.0 m/s to 2.5 m/s. When the ASV gradually increases, the temperature difference between adjacent wind speeds changes slightly. When the ASV increases from 1.5 m/s to 2.0 m/s, the $\overline{\Delta T}$ of the system decreases by about 0.3°C. When ASV increases from 2.5 m/s to 3.0

m/s, the $\overline{\Delta T}$ decreases by about 0.1°C.

3.3.3 Effect of the phase change temperature

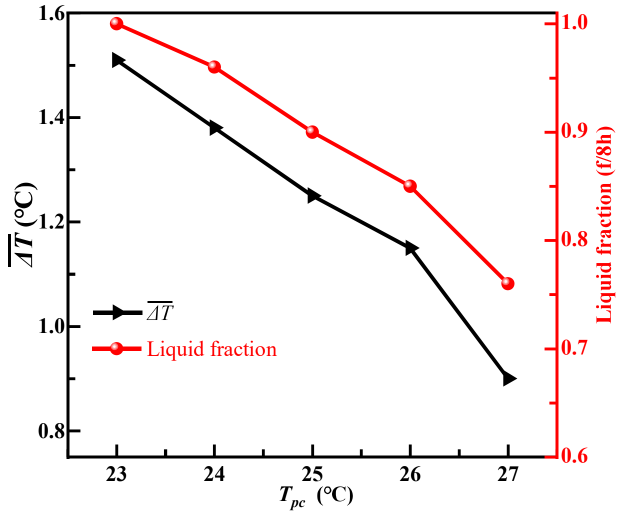

Fig .17. The influence curve of the PCT

PCT is an important factor in PCES's management of storage and release, which affects the storage efficiency and service life of the system. Fig .17 plots the $\overline{\Delta T}$ and liquid fraction of the system at the IAT of 30°C, the ASV of 2 m/s, and a PCT of 23°C, 24°C, 25°C, 26°Cand 27°C, respectively. The $\overline{\Delta T}$ and liquid fraction of the system show a nonlinear decreasing trend with the increase of PCT. When the PCT is 23°C, the $\overline{\Delta T}$ and liquid fraction of the system are the largest, and the liquid fraction is the maximum 1, and the PCP is completely melted. Under the above conditions, PCP with PCT of 23°C per meter can be cooled by an average of 1.5°C. The $\overline{\Delta T}$ and the liquid fraction decrease dramatically at a PCT of 27°C. Compared with PCT of 23°C and 27°C, the liquid fraction decreases by 0.24, dropping 24%; the $\overline{\Delta T}$ decreases by 0.6°C, dropping 40%. Because when the temperature of the heat exchange fluid is constant, the higher PCT reduces the temperature difference between the PCM and the heat exchange flow, and may not absorb enough heat during heat absorption. The upper limit of the allowable supply air temperature in the server room shall not exceed 27°C. Therefore, the PCT of PCES used in data center cooling system should be lower than 27°C.

And the PCT that is too low may result in an inadequate phase change process and ineffective release of heat. The highest temperature at night in Gui'an is about 25°C, the lowest temperature is about 18.6 °C in summer, and the average temperature is 20°C. To ensure that the system can be effectively applied in the data centers of Gui'an, the reasonable PCT range is 25°C-26°C.

3.3.4 Effect of the PCM's thermal conductivity

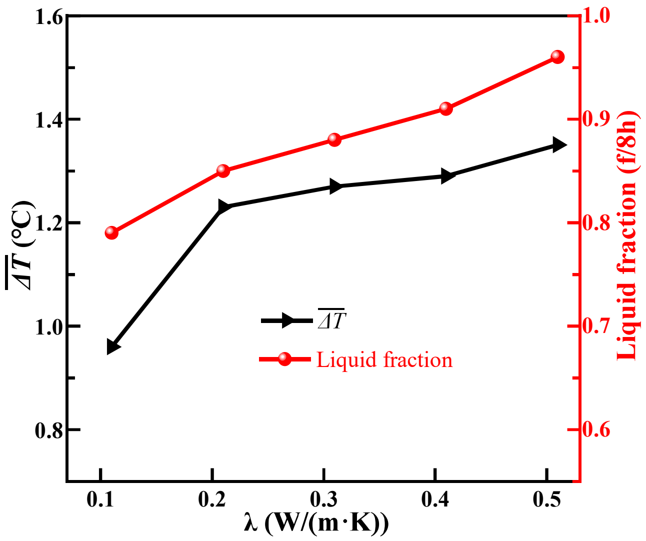

Fig .18. The influence curve of λ

Fig.18 compares the trend of $\overline{\Delta T}$ and the liquid fraction when IAT at 30°C, ASV at 2m/s, PCT is 25.84°C, and λ is 0.11 W/(m·K), 0.21 W/(m·K), 0.31 W/(m·K), 0.41 W/(m·K) and 0.51 W/(m·K), respectively. With the increase of λ, the $\overline{\Delta T}$ of the system first increases rapidly and then slowly increases, and the liquid fraction increases nonlinearly. The growth rates of the $\overline{\Delta T}$ are 28% ,3.3%, 1.6%and 4.7%, respectively. According to Fourier's law, the thermal resistance (R), $R = \frac{\delta}{\lambda A}$, is inversely proportional to the λ during heat conduction. An increase in λ results in a reduction of the R of the PCM. Heat transfer within the PCP mainly occurs through conduction, thus, a lower R facilitates the transfer of heat between the PCM. Additionally, paraffin molecules can readily acquire sufficient energy for phase change, leading to a high f. The λ is 0.21 W/(m·K), the $\overline{\Delta T}$ of the system is about 1.2°C, and the liquid fraction is 0.85. The λ of paraffin wax is usually at 0.2 W/(m·K). The increase of λ has a great effect on the λ. When λ increases from 0.21 W/(m·K) to 0.51 W/(m·K), the $\overline{\Delta T}$ of the system increases by 0.1°C, and the liquid fraction increases by 0.11.

4. Discussions

4.1 Analysis of the value engineering

To obtain the best comprehensive benefits of the system and achieve the necessary functions of the system at the lowest life cycle cost. The value engineering is analyzed based on the following formula (considering product value, functionality, and cost as a whole).

$$\boldsymbol{V} = \frac{\mathbf{F}}{\mathbf{C}} \tag{6}$$

Where: V is the value coefficient; F is the function coefficient, F = the performance weight score of each scheme system / the total score of the two scheme systems; C is the cost factor, C = the cost of each scheme system / the total cost of the scheme systems.

The function of the system is to cool down servers in an energy-efficient manner. According to ASHRAE TC9.9, the maximum allowable air supply temperature of the data center is 27°C, and the mechanical cooling energy savings of the data center air conditioning system can be calculated using Eq. (7).

$$\boldsymbol{\eta} = \frac{\sum_{i=1}^{n}(T_i-27)t_i - \sum_{i=1}^{n}(T_i-27-\Delta T)t_i}{\sum_{i=1}^{n}(T_i-27)t_i} \times \mathbf{100\%} \tag{7}$$

Where: η is the energy saving rate (%); T_i is the air temperature (°C); t_i is the time when mechanical refrigeration is used (h).

The temperature data of Gui'an in 2024 is used to calculate the η. As can be seen from Fig .19, the average annual temperature in Gui'an is low, with the highest temperature of 34.3°C. Temperatures above 27°C are concentrated in July, August, September and October. According to the Fig .19, the total time of the temperature exceeding 27°C in this region is 472 h, accounting for about 5.39% of the total time of the year. The largest proportion of the excess temperature range is 27°C-28°C, with 178 h. Under the same meteorological and environmental conditions, the η of the system application in the preliminary experiment is 61%, and the η of the optimized system is 83%.

According to the feedback from the user experience questionnaire of the data center in Gui'an. A full score of 10 points is used as the standard: 5 points for the cooling function of the pre-optimization system and 5.5 points for energy saving; 6.5 points for the cooling function and 8 points for energy saving of the optimized system. The main functions of optimization in this study are efficient cooling and energy saving, both of which are equally important. Therefore, the cooling capacity and energy-saving capacity are given the same weight, accounting for 0.5 each. The F of the old system is 0.43, and the F of the optimized system is 0.57.

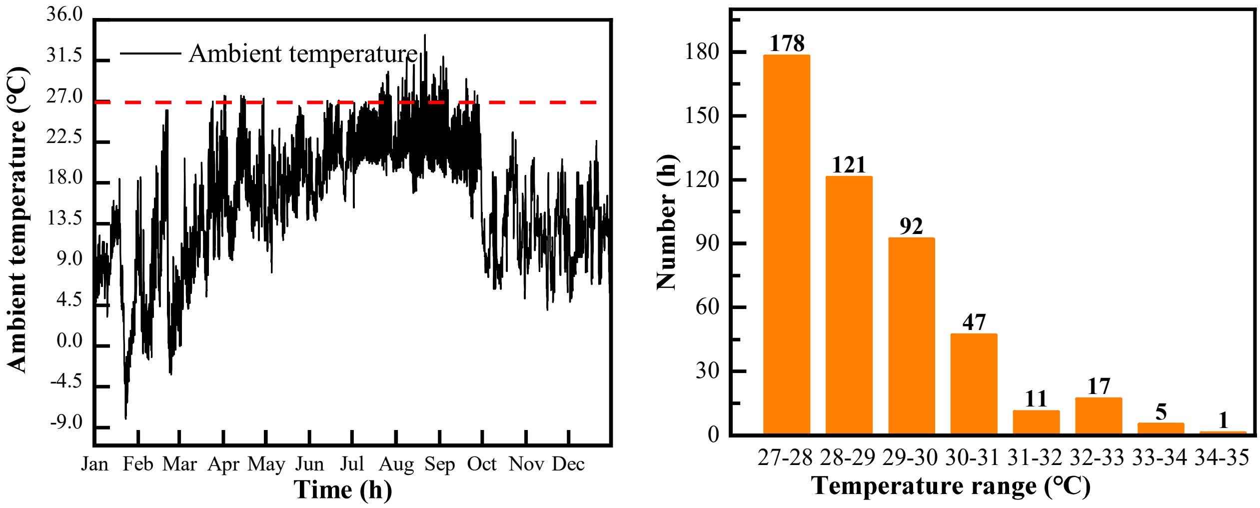

(a) Temperature changes of year (b) The number of h when the temperature exceeds 27°C

Fig .19. Trend of air temperature change in Gui'an in 2024

The cost of the system includes the cost of production and the cost of use. The production cost mainly refers to the materials and equipment to be consumed, including PCM with a unit price of ¥30 /kg, steel plates with a material and processing fee of ¥200/piece, and axial fans with a unit price of

¥20 /piece. Optimized PCP has added accessories, so the materials and processing fee have increased by about ¥260 /block. The cost of use exists in the risk of material leakage in the encapsulated PCP, which requires regular maintenance and overhaul.

Considering the function and cost of the system before and after optimization, the results of the system product value analysis are shown in Table 4. According to the value engineering theory, the design scheme with the largest V is the optimal scheme, and the optimal system is the optimized new system. In this study, the optimization cost increases slightly, and the function increases significantly, which is an investment enhancement value. The V of the optimized system is close to 1 at 1.05, which means that the price matches the performance, quality and function of the product. It has strong market competitiveness and can be widely accepted by the market.

Table 4

Value engineering analysis of system optimization

System	Cost (¥ Ten thousand)	C	η	F	V
Pre-optimization system	1.09	0.45	61%	0.43	0.93
Optimized system	1.35	0.55	83%	0.57	1.05
Change	+ 0.30	+0.1	+22%	+0.14	+0.12

4.2 Analysis of the practical application of the system

The main requirements for the cooling system in the data center environment include strong cooling capacity, small enthalpy difference and large air volume to ensure reliable operation. The previous research discussion shows that the optimized PCP effectively assists with free cooling and reduces the cooling energy consumption of the data center. To facilitate the production design of the system equipment in the data center, the influence equation between the average cooling performance of the optimized system and environmental factors such as the IAT, ASV, PCT, and the λ are further discussed.

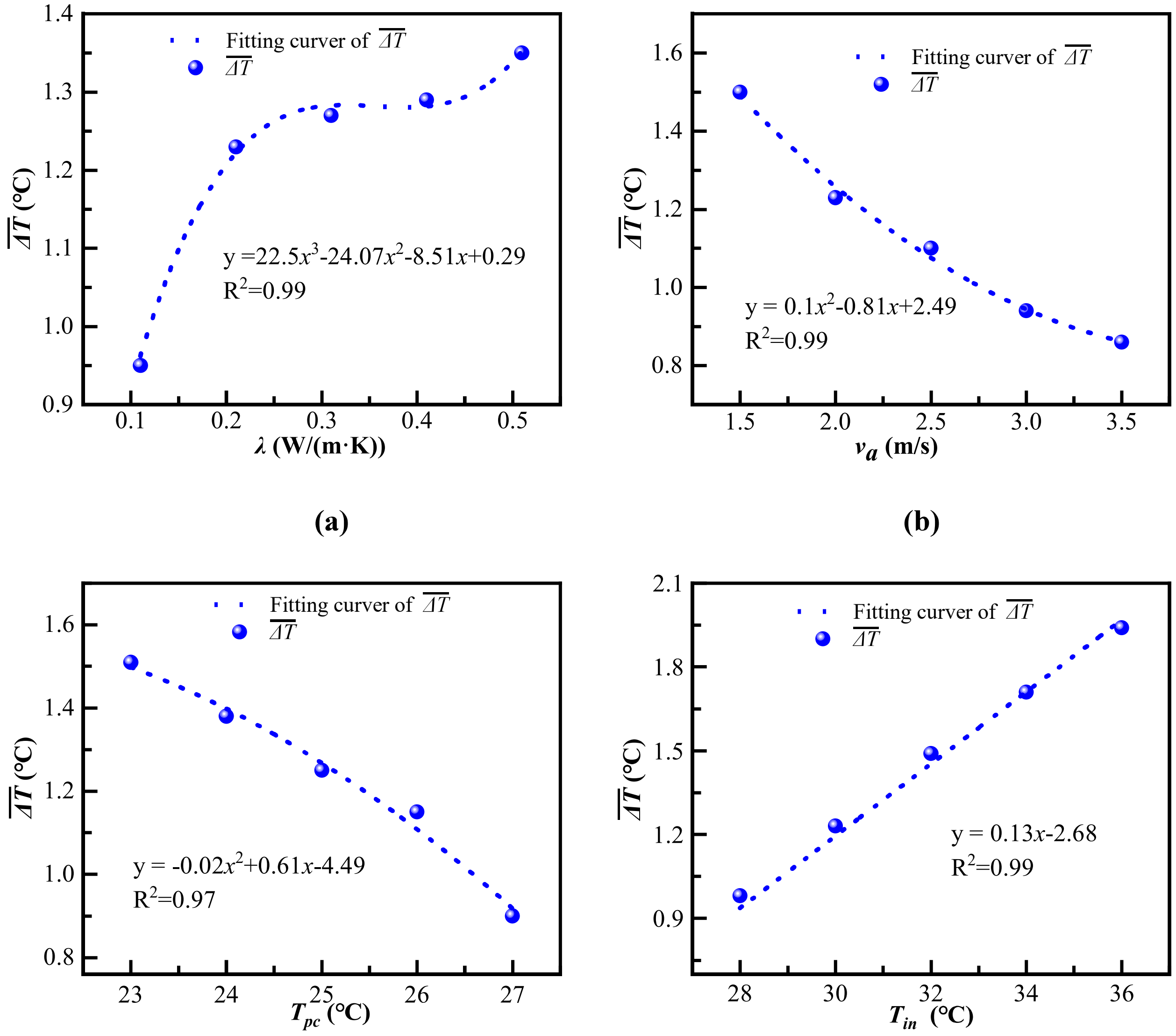

(a) (b)

(c) (d)

Fig .20. Fitting curves of average temperature drop: (a) λ; (b) ASV; (c) PCT; (d) IAT

From Fig .20 can be observed that the $\overline{\Delta T}$ exhibits a strong linear relationship with the IAT, a quadratic functional relationship with the ASV and the PCT, and a cubic functional relationship with the λ. And the R^2 of these four fitting equations are all greater than 0.97. Therefore, the mathematical relationship between $\overline{\Delta T}$ and these four factors can be respectively assumed as:

$$\overline{\Delta T} = f(\lambda, V_a, T_{pc}, T_{in}) = a\lambda^3 + b\lambda^2 + c\lambda + d\, V_a^2 + e\, V_a + f\, T_{pc}^2 + g T_{pc} + h\, T_{in} + i \quad (9)$$

Where $\overline{\Delta T}$ is the average temperature drop of the system (°C); λ is thermal conductivity

(W/(m·K)); V_a is the air supply velocity of the system (m/s); T_{pc} is phase change temperature of PCM (°C); *a*, b, *c*, *d*, *e*, *f*, *g*, *h* and *i* is the model parameters.

Substitute the $\overline{\Delta T}$ values at different IAT, ASV, PCT and the λ in Table 3 into the Eq (9). Through regression analysis, within the 95% confidence interval, the nine coefficients from *a* to *i* were solved. Then the mathematical relationship between $\overline{\Delta T}$ and the four variables is as follows:

$$\overline{\Delta T} = f(\lambda, V_a, T_{pc}, T_{in}) = 17.85\lambda^3 - 19.54\lambda^2 + 7.23\lambda + 0.14V_a^2 - V_a - 0.03T_{pc}^2 + 1.38T_{pc} + 0.13T_{in} - 17.51 \quad (10)$$

According to this quantitative relationship to assess the cooling performance of the trapezoidal PCP system applying in different temperature zones. It establishes a model that links cooling performance of PCP with climatic parameters, so a certain extent of selection can be made for the PCT and the λ of PCM based on specific regional cooling demands and climatic characteristics. Additionally, this relationship provides theoretical grounds for optimized system operating parameters, including setting the PCT threshold and controlling the flow rate of the cooling medium, among key operational indexes that ensure the best cooling efficiency under targeted climatic conditions.

5. Conclusions

Integration of free cooling with PCES enhances energy conservation of data centers. However, the uneven melting of the PCP leads to low conversion energy efficiency. This study numerically investigates structure and configuration of the PCP. The effects of T_{in}, ASV, PCT and λ on the optimized system are studied to provide a design basis for the application of the trapezoidal cavity PCP in ventilation systems. The main conclusions of this paper are as follows:

(1) When the PCP changes from a rectangular cavity to a trapezoidal cavity, the uniformity of

melting is improved by 93% and effectively shorts the charging time of the PCP from 14 h to 11.6 h.

(2) The optimal structure of the trapezoidal cavity PCP in the system is a W_r of 1.5, a horizontal parallel arrangement of double fins in the PCP, and a PCP volume of 19 L. The optimized system increases the average cooling range by about 0.5°C and achieves a 22% increase in energy conservation.

(3) The cooling performance of the PCP increases with the increase of the IAT and λ, and decreases with the increase of ASV and PCT. A nonlinear functional relationship between the average cooling performance of the system and the main four variables is proposed.

This work presents a systematic investigation into the structural and parameters of PCP assisted ventilation system of data center under constant working conditions. This research provides the theoretical guidance for the design of PCES assisted free cooling of ventilation systems. However, there exists a shortcoming between the charging and discharging performance of the PCP and the surrounding ambient temperature. In the future, the impact of real-time and dynamical changes in environmental temperature on the performance of PCP will be studied.

Credit author contribution statement

Hongli Xu: Investigation, Writing - Original Draft. **Jiri Zhou:** Writing - Review & Editing. **Xing Liang:** Methodology. **Hongwei Wu:** Writing - Review & Editing. **Ruiyong Mao:** Conceptualization, Project administration. **Zujing Zhang:** Writing - Review & Editing.

Declaration of Competing Interest

The authors declare that they have no known competing financial interests or personal relationships that could have appeared to influence the work reported in this paper.

Acknowledgments

The author would like to thank the financial support of the National Natural Science Foundation of China (NO.52168013), the Guizhou Provincial Science and Technology Projects (NO. ZK [2022]151) and the Guizhou Province Postgraduate Research Fund Project (NO. 2024YJSKYJJ114).

Reference

[1] Z. Wang, H. Ding, L. Lei, N. Li, W.-Q. Tao, Numerical simulation on the flow and heat transfer characteristics in dimple/protrusion enhanced air handling unit in data center, International Communications in Heat and Mass Transfer 157 (2024) 107710. https://doi.org/10.1016/j.icheatmasstransfer.2024.107710.

[2] L. Ge, Z. Han, Z. Yang, Y. Zhang, B. Qiu, X. Li, Feasibility investigation on a novel data center cooling system based on cross-seasonal soil cool storage in severe cold area, Journal of Energy Storage 98 (2024) 113233. https://doi.org/10.1016/j.est.2024.113233.

[3] E. Masanet, A. Shehabi, N. Lei, S. Smith, J. Koomey, Recalibrating global data center energy-use estimates, Science 367 (2020) 984–986. https://doi.org/10.1126/science.aba3758.

[4] H. Zhu, D. Zhang, H.H. Goh, S. Wang, T. Ahmad, D. Mao, T. Liu, H. Zhao, T. Wu, Future data center energy-conservation and emission-reduction technologies in the context of smart and low-carbon city construction, Sustainable Cities and Society 89 (2023) 104322. https://doi.org/10.1016/j.scs.2022.104322.

[5] F. Bai, X.-M. Gong, H.-W. Li, H.-B. Guo, W.-Q. Tao, An improved black box model and the details of its numerical treatments for rack in data center simulation, International Communications in Heat and Mass Transfer 158 (2024) 107916. https://doi.org/10.1016/j.icheatmasstransfer.2024.107916.

[6] R. Mao, H. Wu, C. Li, Z. Zhang, X. Liang, J. Zhou, J. Chen, Experimental investigation on the application of cold-mist direct evaporative cooling in data centers, International Journal of Thermal Sciences 208 (2025) 109500. https://doi.org/10.1016/j.ijthermalsci.2024.109500.

[7] I. Keskin, G. Soykan, Distribution grid electrical performance and emission analysis of combined cooling, heating and power (CCHP)-photovoltaic (PV)-based data center and residential customers, Journal of Cleaner Production 414 (2023) 137448. https://doi.org/10.1016/j.jclepro.2023.137448.

[8] A novel concept for performance enhancement of immersion-cooled data center servers, International Communications in Heat and Mass Transfer 159 (2024) 107980. https://doi.org/10.1016/j.icheatmasstransfer.2024.107980.

[9] X. Zhou, Z. Xin, W. Tang, K. Sheng, Z. Wu, Energy, economic and environmental analysis of a combined cooling, power generation, and energy storage system: A case study of data center in Shenzhen, Journal of Energy Storage 97 (2024) 112968. https://doi.org/10.1016/j.est.2024.112968.

[10] C. Liu, N. Hao, T. Zhang, D. Wang, Z. Li, W. Bian, Optimization of data-center immersion cooling using liquid air energy storage, Journal of Energy Storage 90 (2024) 111806. https://doi.org/10.1016/j.est.2024.111806.

[11] M.S.K. Tareen, A.F. Zueter, M. Zolfagharroshan, M. Xu, A.P. Sasmito, Seasonal ground cold energy storage potential for data center cooling using thermosyphon: A comparative study of five cities in Canada for carbon footprint reduction, Journal of Energy Storage 84 (2024) 111486. https://doi.org/10.1016/j.est.2024.111486.

[12] C. Wang, H. Yu, L. Xian, G. Liu, L. Chen, W.-Q. Tao, Study on the operation strategy of the water cooling system in the single-phase immersion cooling data center considering cooling tower performance, Energy and Buildings 324 (2024) 114890. https://doi.org/10.1016/j.enbuild.2024.114890.

[13] L. Silva-Llanca, C. Ponce, E. Bermúdez, D. Martínez, A.J. Díaz, F. Aguirre, Improving energy and water consumption of a data center via air free-cooling economization: The effect weather on its performance, Energy Conversion and Management 292 (2023) 117344. https://doi.org/10.1016/j.enconman.2023.117344.

[14] Q. Zhou, R. Mao, L. Wu, J. Chen, J. Zhou, Z. Zhang, Study on multi-scale thermal management optimization for the configuration of a free cooling fan wall data center, Applied Thermal Engineering 265 (2025) 125573. https://doi.org/10.1016/j.applthermaleng.2025.125573.

[15] L. Geng, K Luo, Y Lin, G Li, Y Cao, J. Zhao, C. Liu. Facile Ester-based Phase Change Materials Synthesis for Enhanced Energy Storage Toward Battery Thermal Management. Advanced Science 129 (2025) 2413703. https://doi: 10.1002/advs.202413703.

[16] Z.-X. Wang, Z.-Q. Li, N. Li, P. He, L. Chen, W.-Q. Tao, Numerical simulation of a hybrid energy system proposed for low carbon data center, Applied Thermal Engineering 258 (2025) 124522. https://doi.org/10.1016/j.applthermaleng.2024.124522.

[17] C. Li, R. Mao, Y. Wang, J. Zhang, J. Lan, Z. Zhang, Experimental study on direct evaporative cooling for free cooling of data centers, Energy 288 (2024) 129889. https://doi.org/10.1016/j.energy.2023.129889.

[18] C. Fan, B. Zou, Y. Liao, X. Zhou, Evaluation of energy performance and ecological benefit of free-cooling system for data centers in worldwide climates, Sustainable Cities and Society 108 (2024) 105509. https://doi.org/10.1016/j.scs.2024.105509.

[19] M. Temiz, I. Dincer, A unique bifacial PV and hydrogen-based cleaner energy system with heat recovery for data centers, Applied Thermal Engineering 206 (2022) 118102. https://doi.org/10.1016/j.applthermaleng.2022.118102.

[20] N. Wang, Y. Guo, C. Huang, S. Shao, Advances in direct liquid cooling technology and waste heat recovery for data center: A state-of-the-art review, Journal of Cleaner Production 477 (2024) 143872. https://doi.org/10.1016/j.jclepro.2024.143872.

[21] A. Bahlekeh, H.R. Mouziraji, H. Togun, A.E. Tiji, A.M. Abed, H.I. Mohammed, R.K. Ibrahem, M.S. Alhassan, P. Talebizadehsardari, Evaluation of the solidification process in a double-tube latent heat storage unit equipped with circular fins with optimum fin spacing, Energy Science & Engineering 11 (2023) 2552–2570. https://doi.org/10.1002/ese3.1473.

[22] S.J. Malode, N.P. Shetti, Thermal energy storage systems using bio-based phase change materials: A comprehensive review for building energy efficiency, Journal of Energy Storage 105 (2025) 114709. https://doi.org/10.1016/j.est.2024.114709.

[23] R. Wang, L. Geng, X. Zhang, G. Liang, J. Zhao, C. Liu, Synthesis of flexible form stable phase change materials with in-situ formed porous TiO2 for personal thermal management, Chemical Engineering Journal 505 (2025) 159592. https://doi.org/10.1016/j.cej.2025.159592.
[24] B. Huang, Z. Zheng, G. Lu, X. Zhai, Design and experimental investigation of a PCM based cooling storage unit for emergency cooling in data center, Energy and Buildings 259 (2022) 111871. https://doi.org/10.1016/j.enbuild.2022.111871.
[25] G. Priyadarshi, B. Kiran Naik, Experimental study of novel desiccant coated energy exchanger employing PCM – Silica gel working pair for air conditioning and thermal energy storage application, Energy Conversion and Management 321 (2024) 119042. https://doi.org/10.1016/j.enconman.2024.119042.
[26] Z. Ren, Y. Ren, T. Zhou, T. Wang, X. Gao, Z. Yang, Q. Xiong, S. Chen, Y. Xiao, Investigating the dynamic thermal performance of a novel PCM to earth-air heat exchanger: Developing numerical model and comparing thermal performance, Journal of Building Engineering 97 (2024) 110718. https://doi.org/10.1016/j.jobe.2024.110718.
[27] J.-X. Wang, J. Qian, N. Wang, H. Zhang, X. Cao, F. Liu, G. Hao, A scalable micro-encapsulated phase change material and liquid metal integrated composite for sustainable data center cooling, Renewable Energy 213 (2023) 75–85. https://doi.org/10.1016/j.renene.2023.05.106.
[28] X. Yi, H. Xu, R. Mao, H. Wu, X. Gao, J. Zhou, Z. Zhang, Experimental investigation on evaporative cooling coupled phase change energy storage technology for data centers under natural air cooling, International Communications in Heat and Mass Transfer 159 (2024) 108127. https://doi.org/10.1016/j.icheatmasstransfer.2024.108127.
[29] L. Yang, H. Wu, Z. Zhang, R. Mao, J. Zhou, X. Liang, Experimental investigation on application potential of phase change assisted direct ventilation cooling system for Gui'an data center, Applied Thermal Engineering 254 (2024) 123932. https://doi.org/10.1016/j.applthermaleng.2024.123932.
[30] L. Geng, T. Xiao, J. Jiang, K. Luo, Y. Yan, C. Liu, Wide temperature range phase change cold energy storage by using esterification between polyethylene glycol and lauric acid, Chemical Engineering Journal 496 (2024) 154005. https://doi.org/10.1016/j.cej.2024.154005.
[31] N. Zhang, Z. Zhang, J. Li, X. Cao, Performance analysis and optimization of a hybrid battery thermal management system integrating PCM with Chinese knot-shaped liquid cooling plate, International Communications in Heat and Mass Transfer 159 (2024) 108261. https://doi.org/10.1016/j.icheatmasstransfer.2024.108261.
[32] F.L. Rashid, H.I. Mohammed, A. Dulaimi, M.A. Al-Obaidi, P. Talebizadehsardari, S. Ahmad, A. Ameen, Analysis of heat transfer in various cavity geometries with and without nano-enhanced phase change material: A review, Energy Reports 10 (2023) 3757–3779. https://doi.org/10.1016/j.egyr.2023.10.036.
[33] Y. Liang, H. Yang, H. Wang, X. Bao, H. Cui, Enhancing energy efficiency of air conditioning system through optimization of PCM-based cold energy storage tank: A data center case study, Energy 286 (2024) 129641. https://doi.org/10.1016/j.energy.2023.129641.
[34] Y. Zhu, G. Englmair, H. Huang, J. Dragsted, Y. Yuan, J. Fan, S. Furbo, Numerical investigations of a latent thermal energy storage for data center cooling, Applied Thermal Engineering 236 (2024) 121598. https://doi.org/10.1016/j.applthermaleng.2023.121598.
[35] O. Kosdere, Z. Sert, O. Altun, Investigation of thermal performance at forced convection in

plate-fin heat sink, Energy 307 (2024) 132621. https://doi.org/10.1016/j.energy.2024.132621.
[36] M. Boujelbene, H.I. Mohammed, H.Sh. Majdi, R. Babaei-Mahani, P. Talebizadehsardari, A. Rahbari, Melting performance of nano-enhanced phase change materials in a triple-tube heat exchanger with zigzag-shaped tubes, Journal of Energy Storage 67 (2023) 107484. https://doi.org/10.1016/j.est.2023.107484.
[37] P. Shahamat, Z. Mehrdoost, Numerical investigation of performance enhancement in a PCM-based thermal energy storage system using stair-shaped fins and nanoparticles, Applied Thermal Engineering 257 (2024) 124433. https://doi.org/10.1016/j.applthermaleng.2024.124433.
[38] F. Najim, S. Kaplan, H. Mohammed, A. Dulaimi, A. Abed, R. Ibrahem, F. Al-Qrimli, M. Mahmoud, J. Awrejcewicz, W. Pawłowski, Evaluation of Melting Mechanism and Natural Convection Effect in a Triplex Tube Heat Storage System with a Novel Fin Arrangement, Sustainability 14 (2022) 10982. https://doi.org/10.3390/su141710982.
[39] W. Guo, Z. Zhang, H. Wu, L. Ge, X. Liang, R. Mao, Experimental study on cooling and dehumidification performance of an ice storage air conditioner used in underground refuge chamber, International Communications in Heat and Mass Transfer 146 (2023) 106930. https://doi.org/10.1016/j.icheatmasstransfer.2023.106930.
[40] X. Ma, Q. Zhang, S. Zou, An experimental and numerical study on the thermal performance of a loop thermosyphon integrated with latent thermal energy storage for emergency cooling in a data center, Energy 253 (2022) 123946. https://doi.org/10.1016/j.energy.2022.123946.
[41] D. Dubert, B. Šeta, J. Massons, Jna. Gavaldà, M.M. Bou-Ali, X. Ruiz, V. Shevtsova, Enhancing PCM thermal management in multi-cycle melting-solidification, International Communications in Heat and Mass Transfer 157 (2024) 107741. https://doi.org/10.1016/j.icheatmasstransfer.2024.107741.
[42] D.L. Roux, S. Serra, S. Sochard, J.-M. Reneaume, Sensibility analysis and environmental impact of a system combining a solar-assisted heat pump and PCM storages, Energy Conversion and Management 322 (2024) 119108. https://doi.org/10.1016/j.enconman.2024.119108.
[43] Y. Zhao, J. Yu, B. Zhao, Y. Xu, W.-S. Chang, H. Guo, Potential of phase change materials to mitigate overheating in residential blocks in severe cold regions of China, Sustainable Cities and Society 119 (2025) 106114. https://doi.org/10.1016/j.scs.2024.106114.
[44] T. Pirasaci, A. Sunol, Potential of phase change materials (PCM) for building thermal performance enhancement: PCM-composite aggregate application throughout Turkey, Energy 292 (2024) 130589. https://doi.org/10.1016/j.energy.2024.130589.
[45] F.B. Planella, A simple model for latent thermal energy storage systems with encapsulated phase-change material, International Journal of Heat and Mass Transfer (2025).
[46] L. Geng, J. Cui, C. Zhang, Y. Yan, J. Zhao, C. Liu, Chemistry in phase change energy storage: Properties regulation on organic phase change materials by covalent bond modification, Chemical Engineering Journal 495 (2024) 153359. https://doi.org/10.1016/j.cej.2024.153359.
[47] C. Zhao, J. Wang, Y. Sun, S. He, K. Hooman, Fin design optimization to enhance PCM melting rate inside a rectangular enclosure, Applied Energy 321 (2022) 119368. https://doi.org/10.1016/j.apenergy.2022.119368.
[48] X. Liu, X. Qin, Y. Tian, Q. Luo, H. Yao, J. Wang, C. Dang, Q. Xu, S. Lv, Y. Xuan, Biomimetic optimized vertically aligned annular fins for fast latent heat thermal energy storage, Applied Energy 347 (2023) 121435. https://doi.org/10.1016/j.apenergy.2023.121435.

[49] A.A. Al-Abidi, S. Mat, K. Sopian, M.Y. Sulaiman, Abdulrahman.Th. Mohammad, Experimental study of melting and solidification of PCM in a triplex tube heat exchanger with fins, Energy and Buildings 68 (2014) 33–41. https://doi.org/10.1016/j.enbuild.2013.09.007.
[50] L. Liu, Q. Zhang, X. Zhao, A simplified method to simulate tube-in-tank latent thermal energy storage with fin-enhanced phase change material in data center, Journal of Energy Storage (2022).
[51] C.-C. Liao, W.-K. Li, M.-F. Hsieh, Numerical investigation of enhanced PCM melting performance using a thermally conductive fin in a pneumatic-based extrusion system, International Communications in Heat and Mass Transfer 159 (2024) 108311. https://doi.org/10.1016/j.icheatmasstransfer.2024.108311.
[52] P.T. Sardari, H.I. Mohammed, D. Giddings, G.S. Walker, M. Gillott, D. Grant, Numerical study of a multiple-segment metal foam-PCM latent heat storage unit: Effect of porosity, pore density and location of heat source, Energy 189 (2019) 116108. https://doi.org/10.1016/j.energy.2019.116108.